Experimental and theoretical study of bound and quasibound states of Ce^-

C. W. Walter,* N. D. Gibson, Y.-G. Li, D. J. Matyas, R. M. Alton, S. E. Lou, and R. L. Field III
Department of Physics and Astronomy, Denison University, Granville, Ohio 43023, USA

D. Hanstorp
Department of Physics, University of Gothenburg, SE-412 96 Gothenburg, Sweden

Lin Pan† and Donald R. Beck
Department of Physics, Michigan Technological University, Houghton, Michigan 49931, USA
(Received 30 June 2011; published 21 September 2011)

The negative ion of cerium is investigated experimentally with tunable infrared laser photodetachment spectroscopy and theoretically with relativistic configuration interaction in the continuum formalism. The relative cross section for neutral atom production is measured with a crossed ion-beam–laser-beam apparatus over the photon energy range of 0.54–0.75 eV. A rich resonance spectrum is revealed near the threshold with, at least, 12 peaks observed due to transitions from bound states of Ce^- to either bound or quasibound excited states of the negative ion. Theoretical calculations of the photodetachment cross sections enable identification of the transitions responsible for the measured peaks. Two of the peaks are due to electric dipole-allowed bound-bound transitions in Ce^-, making cerium only the second atomic negative ion that has been demonstrated to support multiple bound states of opposite parity. In addition, combining the experimental data with the theoretical analysis determines the electron affinity of cerium to be 0.628(10) eV and the fine structure splitting of the ground state of Ce^- ($^4H_{7/2}$–$^4H_{9/2}$) to be 0.097 75(4) eV.

DOI: 10.1103/PhysRevA.84.032514 PACS number(s): 31.15.am, 32.80.Gc, 32.10.Hq, 31.15.ve

I. INTRODUCTION

Negative ions are of interest for both applied and fundamental reasons [1]. They are important in a variety of physical situations, ranging from plasmas and discharges to atmospheric chemistry. Because the extra electron in negative ions is not bound by a net Coulomb field, electron correlation is a dominant factor in their structure and stability. Thus, studies of negative ions yield key insights into the dynamics of multielectron interactions, serve as important tests for detailed atomic structure calculations, and provide a valuable opportunity to investigate the general problem of many-body interactions.

Among atomic negative ions, the lanthanides are particularly interesting and challenging because the large number of electrons and the presence of several open shells lead to strong valence-valence and core-valence correlation effects [2,3]. Theoretical calculations by O'Malley and Beck [4] predicted that the negative ion of cerium, Ce^-, has multiple bound states of both odd configuration $4f5d^26s^2$ and even configuration $4f5d6s^26p$; Cao and Dolg [5] also calculated multiple bound states of opposite parity. The density of states in Ce^- is unprecedented in atomic negative ions because the shallow polarization potential of the neutral core typically only supports a single bound electronic configuration in most negative ions. In the present paper, electric dipole transitions between two bound states of Ce^- are observed through $5d \rightarrow 6p$ excitations. Such bound-bound transitions have been observed previously for only a single atomic negative ion, Os^- [6–8]. Studies of electric dipole-allowed transitions take on greater importance with the recent propositions to laser cool negative ions [7–11].

A partial energy-level diagram of Ce^- and Ce is shown in Fig. 1, and details of relevant bound states are given in Table I. The ground-state configuration of neutral Ce ($Z = 58$) has a primary LS character ([Xe] $4f5d6s^2\ ^1G_4$) [12], and the ground state of the negative ion is formed by the addition of a $5d$ electron to produce Ce^- ([Xe] $4f5d^26s^2\ ^4H_{7/2}$) [13]. Recent theoretical calculations of the electron affinity of Ce, corresponding to the binding energy (BE) of the ground state of Ce^-, range from 0.511 eV [14] to 0.61 eV [15]. Experimentally, laser photodetachment electron spectroscopy (LPES) of Ce^- was used by Davis and Thompson to determine a value for the electron affinity of 0.955(26) eV [16]. However, a subsequent reinterpretation of the LPES data based on comparisons to theoretical calculations of photodetachment cross sections yielded an electron affinity of 0.660 eV [14], which is substantially lower than the original LPES value [16] but is consistent with previous *ab initio* theoretical values [5,13,15].

To help resolve this discrepancy between prior experimental and theoretical results, we previously used tunable laser photodetachment threshold (LPT) spectroscopy to measure the threshold energy for the opening of the Ce^- ($^4H_{7/2}$) to Ce ($^1G_4$) ground-state to ground-state transition [17]. The resulting measured value for the electron affinity of Ce was 0.65(3) eV [17], confirming the much lower binding energies predicted by theoretical calculations [5,13,15]. Our previous LPT paper [17] further revealed the existence of, at least, five narrow resonance peaks in the near-threshold region between 0.618 and 0.700 eV.

In the present paper, we have extended the measurements of photodetachment from Ce^- to the energy range of

*walter@denison.edu
†Present address: Department of Science and Mathematics, Cedarville University, Cedarville, OH 45314, lpan@cedarville.edu

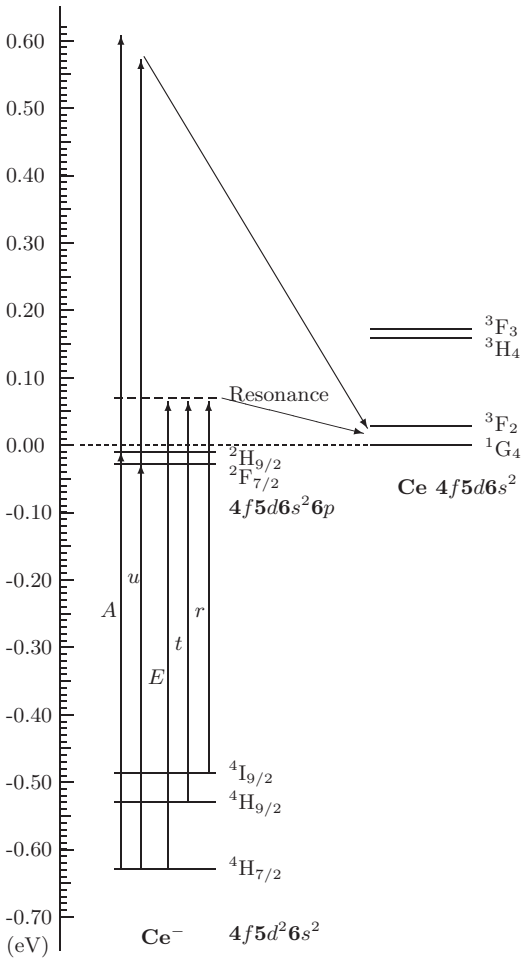

FIG. 1. Partial energy diagram for relevant levels of Ce^- and Ce. The binding energies are from this paper. The energy values of Ce are taken from Ref. [12], except that the LS of the lowest $J = 3$ level has been corrected by relativistic configuration-interaction (RCI) calculations performed in this paper. The arrows indicate the two-step resonant detachment process used to observe bound-bound transitions and examples of the single-photon direct detachment process used to observe quasibound resonances. To the left of each arrow is the label used in this paper for the peak corresponding to each process.

0.54–0.75 eV and have observed and have characterized seven additional resonance peaks. Theoretical calculations have been performed of photodetachment cross sections, including bound and quasibound excited states of Ce^- over this energy range, enabling identification of the transitions responsible for all 12 of the observed peaks. Two of the peaks were found to be due to bound-bound transitions, detected here through a two-step process of single-photon excitation followed by photodetachment. The results yield a more precise value for the electron affinity of Ce of 0.628(10) eV and determine the fine structure splitting of the ground state of Ce^- ($^4H_{7/2}$–$^4H_{9/2}$) to be 0.097 75(4) eV.

TABLE I. Binding energies (eV) and leading LS compositions (%) of Ce^- bound states relevant to this paper.

Bound state and leading LS terms[a]	Binding energy	
	O'Malley and Beck [4]	This paper
Ce^- $4f5d^26s^2$		
$^4H_{7/2}$ 73%, ^{2}G 26%	0.660	0.628
$^4H_{9/2}$ 64%, ^{2}G 31%	0.560	0.530
$^4I_{9/2}$ 92%	0.516	0.486
Ce^- $4f5d6s^26p$		
$^2F_{7/2}$ 41%, ^{4}H 35%, ^{4}G 13%	0.028	0.028
$^2H_{9/2}$ 40%, ^{2}G 30%, ^{4}I 23%	0.018	0.010

[a]Taken from Tables VIII and IX in Ref. [4]. A cutoff of 10% is applied to the LS compositions to show only the leading LS terms.

II. EXPERIMENTAL METHOD AND MEASURED SPECTRUM

In the present paper, the relative cross section for photodetachment from Ce^- was measured as a function of photon energy using a crossed ion-beam–laser-beam system. The experimental system has been described in detail elsewhere [18], so only a brief description will be given here. The main difference from our previous study on Ce^- [17] is that a new laser system and a higher precision wave meter were used in the present experiment. The new laser system permits continuous scanning of the wavelength, and it was used together with a new data acquisition method that recorded both wavelength and energy data for each individual laser pulse. This is in contrast to our previous method in which the wavelength was moved in fixed wavelength steps and only the average data for multiple shots were recorded. Thus, this new system enables better measurements of narrow peaks in the photodetachment spectrum.

Negative ions were produced by a cesium sputtering source using a cathode packed with CeO_2 powder and then covered with tungsten in a double-layer design [19]. The ions were accelerated to 12 keV, and the $^{140}Ce^-$ isotope was then mass selected using a 90° focusing sector magnet to steer the beam into a UHV chamber. In the interaction region, the ion beam was intersected perpendicularly by a pulsed laser beam. Following the interaction region, residual negative ions in the beam were electrostatically deflected into a Faraday cup to monitor the ion current; typical ion beam currents of $^{140}Ce^-$ were 0.1 nA. Neutral atoms continued undeflected to strike a multidynode electron multiplier detector.

The output from the detector was recorded as a function of time after each laser pulse using a digital storage oscilloscope. The oscilloscope functioned effectively as a time-gated integrator: The detector voltage was integrated over the arrival window corresponding to the flight time of photodetached neutral Ce atoms from the interaction region to the detector. The background was subtracted from this integrated voltage to obtain a signal proportional to the number of neutral atoms produced by each laser pulse. The ion-beam current, the laser wavelength, and the laser-pulse energy were measured for each shot. The neutral atom signal was then normalized to the ion-beam current and the laser photon flux to obtain the relative cross section for photodetachment. Spectra were built up by repeatedly scanning the laser wavelength over the range of interest in continuous scans then sorting the data into photon energy bins of selectable width. Tests were conducted to ensure the linearity of the photodetachment and detection system.

The laser system consisted of a tunable optical parametric oscillator-amplifier (OPO-OPA) (LaserVision) pumped by a

pulsed injection-seeded neodymium-doped yttrium aluminum garnet (Nd:YAG) laser (Continuum) operating at 20 Hz. The fundamental output of the Nd:YAG laser was doubled to pump an optical parametric oscillator (OPO) crystal, producing signal light in the near-infrared (NIR) over the range of 710–880 nm and idler light from 1350 to 2100 nm. The OPO idler light was then used to seed a four-crystal optical parametric amplifier (OPA) system pumped by the Nd:YAG fundamental, producing amplified OPA signal light over the range of 1350–2100 nm and OPA idler light over the range of 2100–5000 nm. The vacuum wavelengths of the NIR light and both the Nd:YAG fundamental and doubled outputs were measured with a pulsed wave meter (HighFinesse GmbH WS6-600) that could operate over the range of 350–1120 nm. The photon energy of the OPA signal light (E_S) was calculated based on conservation of energy by subtracting the measured NIR photon energy (E_{NIR}) from the measured doubled Nd:YAG photon energy [$E_D = 2.329\ 56(1)$ eV],

$$E_S = E_D - E_{\mathrm{NIR}}. \tag{1}$$

The photon energy of the OPA idler light (E_I) was then determined by subtracting the OPA signal photon energy from the measured Nd:YAG fundamental photon energy [$E_F = 1.164\ 78(1)$ eV],

$$E_I = E_F - E_S. \tag{2}$$

In the present experiments, the OPA signal light was used to measure all of the transitions with the exception of the two lowest photon energy transitions (peaks r and s), which were measured with the OPA idler light. The energy per laser pulse in the interaction region was typically in the range of 0.05–0.1 mJ with a pulse duration of 5–7 ns. The effective full bandwidth of the light was $\sim$0.01 meV.

The relative photodetachment spectrum of Ce^- measured in the present paper from 0.540 to 0.615 eV is shown in Fig. 2; also included in the figure are data from our previous paper [17] covering the photon energy range of 0.615–0.750 eV. The spectrum consists of a slowly varying continuum component with a number of prominent peaks superimposed. The flat continuum signal below $\sim$0.65 eV is due to photodetachment from weakly bound ions, with a gradual rise above $\sim$0.65 eV due to the opening of detachment from the Ce^- ($^4H_{7/2}$) ground state to the two lowest neutral Ce states ($^1G_4$ and $^3F_2$).

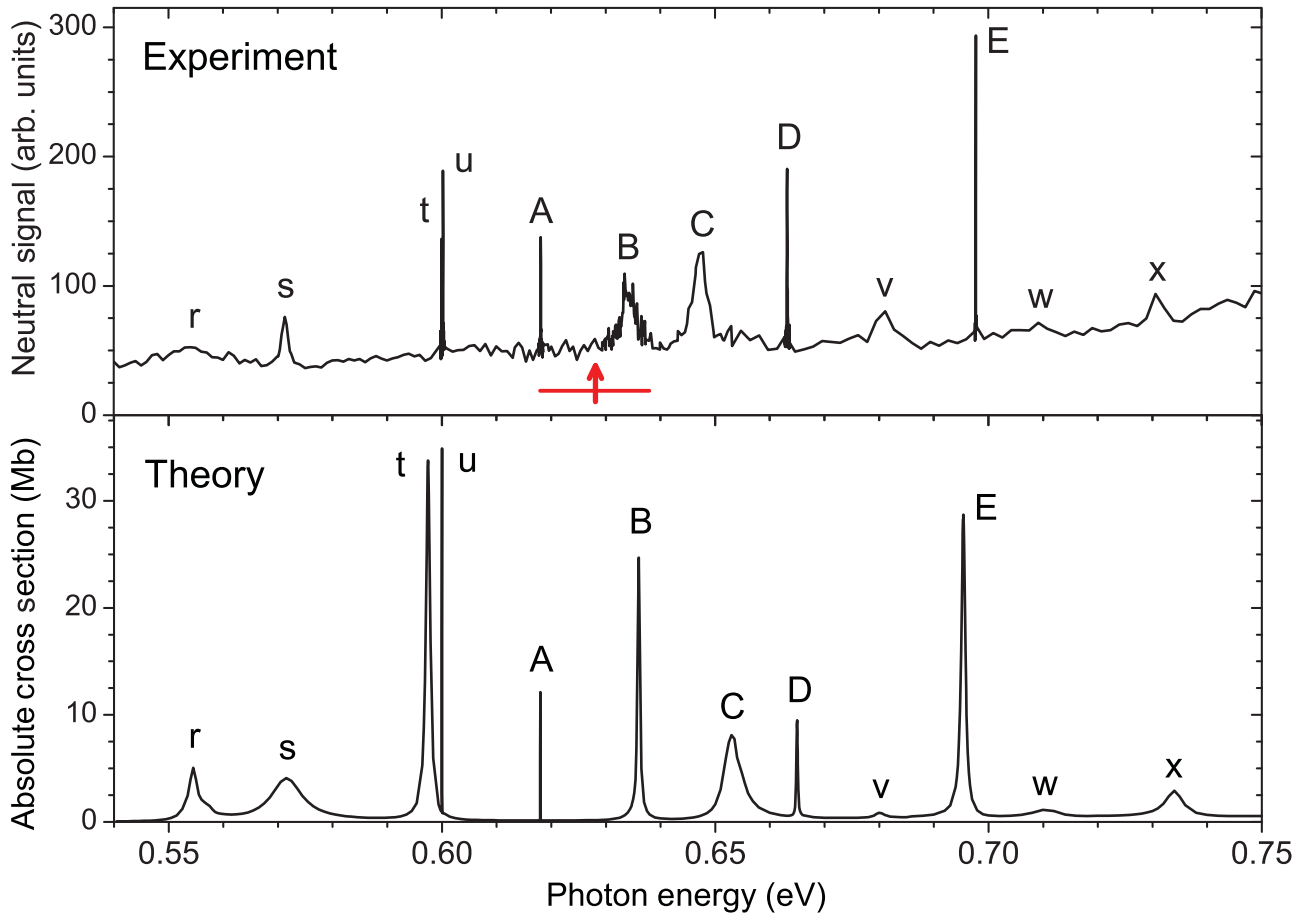

FIG. 2. (Color online) Measured and calculated photodetachment spectra. (Top panel) Measured normalized neutral production signal for photodetachment from Ce^-. The threshold for photodetachment from $^4H_{7/2}$ is indicated by the arrow with uncertainty shown by the horizontal bar. Twelve resonance peaks are labeled with letters; peaks t and u are not resolvable on this scale (see Fig. 3 for an expanded view of these two peaks). The data above 0.615 eV are from Walter *et al.* [17], shifted 0.37 meV lower in energy as discussed in the text. (Bottom panel) Calculated photodetachment cross section of Ce^- from initial states $^4H_{7/2}$, $^4H_{9/2}$, and $^4I_{9/2}$. Multiplicative Boltzmann factors based on effective temperature $T = 650$ K are used when summing the cross sections from all three states.

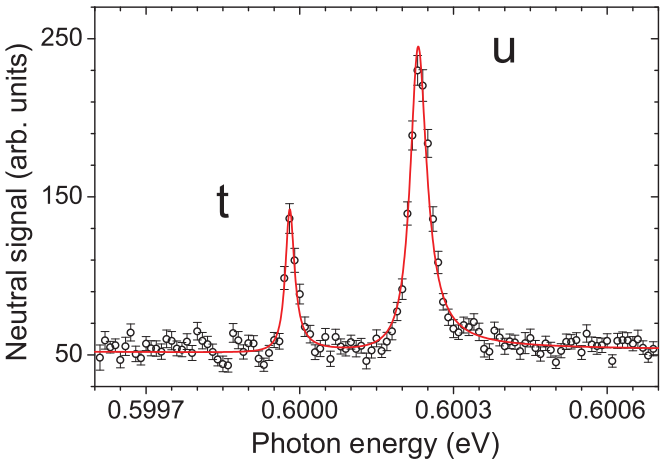

FIG. 3. (Color online) Measured normalized neutral production signal for photodetachment from Ce^- in the vicinity of peaks t and u. Open circles, measured data; solid line, fit of the Fano function [Eq. (3)] to the data.

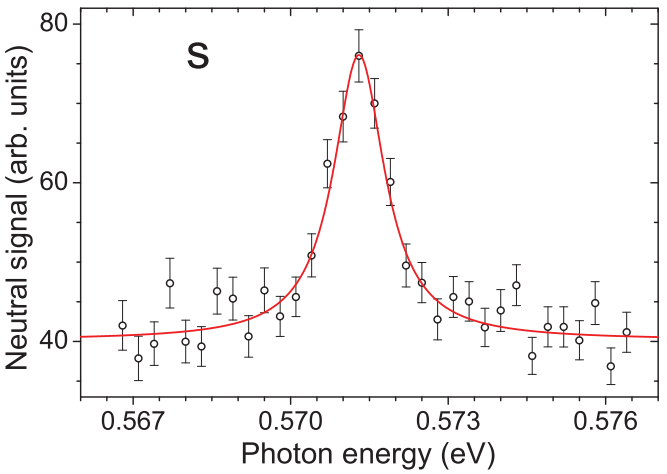

FIG. 4. (Color online) Measured normalized neutral production signal for photodetachment from Ce^- in the vicinity of peak s. Open circles, measured data; solid line, fit of the Fano function [Eq. (3)] to the data.

At least 12 resonance peaks are observed over the photon energy range of 0.54–0.75 eV. It should be noted that there may be additional very narrow, weak, or overlapping photodetachment peaks in this energy range that are not apparent in the measured spectrum due to resolution and/or signal-to-noise limitations in the present experiments. Peaks in the photodetachment spectrum may be either due to single-photon transitions to quasibound excited states of the negative ion that subsequently autodetach or due to transitions to bound excited states that are observed by a two-step process: The first photon excites the negative ion to the upper state, which then absorbs a second photon to detach an electron.

To determine the peak energies and widths, Fano profiles [20] were fit to the peaks. The Fano formula gives the cross section in the vicinity of the peak as

$$\sigma = \sigma_0 + b\frac{(q+\varepsilon)^2}{1+\varepsilon^2}, \tag{3}$$

where σ_0 is the continuum cross section (assumed constant over the narrow energy ranges of the peak fits in the present case), q is the line-shape parameter, and b is a scaling constant. The factor ε is given by $(E - E_r)/(\Gamma/2)$, where E is the photon energy, E_r is the energy of the resonance, and Γ is the peak width (dependent on the lifetime of the excited state). The fitted curves are included with the measured spectra for peaks u, t, and s in Figs. 3 and 4; similar figures for peaks A–E are shown in Ref. [17]. The resonance energies and widths obtained by fitting Eq. (3) to the measured peaks are listed in Table II. The uncertainties are given as 1-standard deviation (1-SD) of the uncertainties of the fitting parameters. For the resonance energies, the fitting uncertainty is added in quadrature with the 1-SD uncertainty in the absolute photon energy calibration, which includes possible Doppler shifts due to deviations from perpendicular incidence. Note that the two narrowest observed peaks, peaks t and E, are somewhat instrumentally broadened by the laser bandwidth of $\sim$0.01 meV.

Three of the peaks observed in our previous paper [17] were remeasured in the present paper using our new higher-precision laser and wave meter system. Peaks A, D, and E were found to be shifted by 0.37 meV lower in energy than reported in our previous paper [17]. This systematic offset was due to a malfunction of the older wave meter used to calibrate the photon energy in the previous experiment. In the present paper, the photon energy calibration was verified by measurements of a stabilized helium-neon laser and a photodetachment threshold of Al^- [18]. The widths of the peaks are not affected by the absolute wave meter calibration, and the widths measured in the present paper are consistent with our previous measurements [17]. Included in Table II, along with the present results, are resonance parameters for five additional peaks

TABLE II. Resonance parameters for peaks measured in photodetachment from Ce^- obtained from fits of the Fano resonance formula [Eq. (3)] to the measured data. The calculated positions of the peaks by RCI are listed; some of the calculated values are averaged over several transitions (see Tables III and IV). All the units are in meV.

Peak	Experiment			Calculation peak energy
	Energy (E_r)	Width (Γ)	Reference	
r	554(1)	14(2)	Present paper	554
s	571.30(6)	1.21(13)	Present paper	571
t	599.98(3)	0.021(5)[c]	Present paper	597
u	600.23(3)	0.039(5)	Present paper	600
A	618.16(3)	0.040(8)	Present paper	618
B	633.8(4)[b]	2.5(5)	[17]	636
C	647.2(4)[b]	2.8(3)	[17]	653
D	663.20(3)	0.099(15)	Present paper	665
v[a]	680.7(5)[b]	3.8(8)	[17]	680
E	697.73(3)	0.018(5)[c]	Present paper	695
w[a]	708(1)[b]	7(4)	[17]	710
x[a]	731.0(5)[b]	2.3(8)	[17]	735

[a]These peaks are weak peaks observed in Ref. [17] that were not previously analyzed (see Fig. 5 of Ref. [17]).
[b]The energies listed in the table for these peaks are shifted 0.37 meV lower than listed in Ref. [17] as discussed in the text.
[c]The widths of these peaks are instrumentally broadened by the laser bandwidth as discussed in the text.

that were observed in our previous paper [17] but were not remeasured in the present paper; the listed energies of these peaks have been shifted 0.37 meV lower to account for the photon energy calibration offset in the previous measurements.

The fitted line-shape parameters q were found to be large ($q > 15$) for all of the observed peaks with the exception of peak B [$q = 7(3)$], indicating that the peaks were quite symmetric. Indeed, fits of the Lorentz function to the peaks yielded energies and widths that were identical within the quoted uncertainties of the values obtained with Fano fits for all of the peaks except for B. This finding of highly symmetric peaks is to be expected for either bound-bound transitions (pure Lorentzian) or for Feshbach resonances embedded in a continuum in which the resonance contribution to the cross section is much stronger than the continuum component, thus, making interference effects minimal. In contrast, the asymmetric profile of peak B is consistent with its identification as a shape resonance positioned just above the ground-state threshold, as discussed in Sec. IV below.

III. THEORETICAL METHOD

Our goal is to identify the observed peaks in the experimental spectrum by comparing them to a theoretically calculated photodetachment cross section spectrum. We will focus primarily on the positions of the peaks rather than on the amplitudes of the peaks, i.e., the absolute cross sections. Because of this, several approximations were made in this paper as will be discussed later.

Throughout the computational part, the quasibound transient states are called resonance states, and the peaks they produce in the photodetachment signal spectrum through interacting with the continuum states are called resonance peaks.

A. Many-electron wave function

All the wave functions for the bound states are calculated using the RCI methodology. Details of it can be found elsewhere [21]. Briefly, the RCI calculation begins by generating the one-electron basis set for orbitals occupied in the reference configurations, e.g., Ce^- $4f5d^26s^2$, using the multiconfiguration Dirac-Fock (MCDF) program of Desclaux [22]. The many-electron wave functions are eigenstates of J^2, J_z, and parity, and are expressed as linear combinations of antisymmetrized determinants of the one-electron basis functions. Correlation is introduced into the wave function by adding configurations that are obtained by replacing one or two electrons in the reference configuration(s). The orbitals that are not occupied in the reference configuration(s) are represented by virtual orbitals. The preorthogonalized radial function for each virtual orbital is in the form of the relativistic screened hydrogenic function with one adjustable parameter, the effective charge (Z^*), which is determined during the energy variational process of RCI.

The wave functions for the three lowest odd states of Ce^- $4f5d^26s^2$—i.e., $^4H_{7/2}$, $^4H_{9/2}$, and $^4I_{9/2}$—have been prepared earlier [4,14]. In this paper, they are regenerated using the valence RCI method. Two sets of virtual orbitals are employed to represent the correlation from replacing one or two valence electrons of $5d$, $6s$. The configuration $4f5d^26p^2$ is found to have a large mixing ($\sim$6% to 7%) in the wave function. Adding correlation to it helps lower the total energy by about 0.033 eV, but the LS compositions remain unchanged.

Given the photon energy range of 0.54–0.75 eV, photodetachment from the above odd states can only access Ce I $4f5d6s^2$ $^1G_4$ and $^3F_2$, and sometimes $^3H_4$ and $^3F_3$ (see Fig. 1). According to the literature [12], the two lowest $J = 3$ states are $^3G_3$ and $^3F_3$, lying 0.172 and 0.206 eV above the $^1G_4$ ground state, respectively. RCI calculations place the lowest $J = 3$ level at the same energy position as in Ref. [12]. However, the identities of the two lowest states are flipped when comparing the LS compositions and Landé g values to Ref. [12]. The lowest $J = 3$ state is actually a $^3F_3$ level. Moreover, the new $^3G_3$ level lies at about 0.4 eV above the $^1G_4$ ground state, which is higher in energy than the accessible range for single-photon detachment in the present paper.

The wave functions for the Ce I states are generated differently from that in Ref. [14]. A common radial set is employed for all the neutral states as well as the Ce^- resonance states $4f5d6s^26p$. The reason behind this will be discussed in Sec. III B. Specifically, the $1s, \ldots, 4f, 5d, 6s$ radial functions are obtained from the MCDF calculation for the Ce I ground state, $4f5d6s^2$ $^1G_4$. These radial functions do not differ substantially between the neutral states and the resonance states. A diffuse numeric $6p$ radial extracted from the MCDF calculation for Ce^- $4f5d6s^26p$ $^2F_{7/2}$ (Table I) is then attached at the end, thus, completing the Dirac-Fock (DF) radial function set. The first set of virtual orbitals is obtained by optimizing the most bound Ce^- $4f5d6s^26p$ $J = 9/2$ state. The virtual orbitals and the DF radial make up the common radial set to all Ce I states and Ce^- resonance states.

Next, in order to compensate for the inadequacy of this common radial set, a second set of virtual orbitals is added that is optimized separately for each individual state. The second set of virtual orbitals contributes trivially to the wave function. For example, a correlation configuration involving a second virtual orbital usually has a coefficient of $\leqslant 0.0005$. Another way to compensate for the inadequacy of the common radial set is to shift the diagonal matrix elements. For the Ce I states, since their energy values are taken from the literature [12], we are only concerned with the proper mixing of the eigenvectors, which is indicated by the Landé g values. Using the radial set described above, the calculated Landé g values for the Ce I $4f5d6s^2$ $^1G_4$, $^3F_3$, and $^3H_4$ levels agree with the experimental values to the second digit after the decimal. The exception is $^3F_2$, whose calculated value is 0.697 while the experimental value is 0.765 [12]—an error of about 9%. Analysis of the composition of the $^3F_2$ level shows it has too little mixing of $^1D_2$ (the Landé g value for a pure $^3F_2$ is 0.666 while the Landé g value for a pure $^1D_2$ is 1.000). The $^1D_2$ lies about 0.17 eV too high above $^3F_2$ at the DF level, using either the common radial set or the specific radial set for $J = 2$. Moreover, the valence-correlation configurations make very little relative difference between $^3F_2$ and $^1D_2$. Separate small calculations indicate the majority of the missing 0.17-eV correlation energy in $^1D_2$ comes from the one-electron replacement of $5s$ by $5d$, vd and $5p$ by $4f$, vf (v stands for virtual orbitals). Since our concern is the $^3F_2$ level only, instead of introducing these (shallow) core-correlation effects into the basis set, we shift down the $^1D_2$ level to its right position. As a result, the Landé g value of

the $^3F_2$ level is increased to 0.764, in good agreement with the experimental value.

The continuum-state wave function is constructed by coupling the wave function of a free electron to that of a neutral state [23]. It is assumed that the wave function of the free electron takes the same angular form as that of a bound electron. Its radial function is numerically generated in a frozen-core DF potential, using a modified version [23] of the relativistic continuum wave solver code of Perger *et al.* [24] and Tews and Perger [25].

B. Photodetachment cross section

The cross section is calculated using [26]

$$\sigma = 4\pi^2 \alpha a_0^2 \frac{df}{dE} = 8.067 \times 10^{-18} \frac{df}{dE}\ (\mathrm{cm}^2), \qquad (4)$$

where α is the fine-structure constant, a_0 is the radius of the first Bohr orbit, and $\frac{df}{dE}$ is the differential oscillator strength for the electric dipole ($E1$) transition from the Ce^- odd bound state to the final continuum state. The $\frac{df}{dE}$ term is evaluated using a modified version [27] of our code for bound states [21,28], the core of which is to compute the transition matrix element. This modified version has been used to successfully reproduce the experimental photoelectron spectrum of Ce^- [14].

Photodetachment cross section calculations without mixing of resonance states show no peak in the 0.54–0.75-eV range. Therefore, the peaks must be due to bound-bound transitions and/or the presence of resonances. To take the effect of resonances into account, Mies's formalism [29] is employed. The procedure and relevant formulas are summarized in our earlier paper on Hf^- [30]. The readers are referred to Refs. [29,30] for the details; here, only those that are necessary to explain the calculation are given. The final state is expressed as a linear combination of the continua $\psi_{\beta E}$'s and resonance states,

$$\Psi_{\alpha E} = \sum_\beta Z_{\alpha\beta} \left(\psi_{\beta E} + \sum_n \frac{v_{n\beta}}{E - \varepsilon_n} \Phi_n \right), \qquad (5)$$

where Φ_n is the modified resonance state that includes an admixture of continuum states and $v_{n\beta}$ is the configuration-interaction (CI) matrix element between the transformed resonance state and the continuum state. The total photodetachment cross section into all channels is

$$\sigma_E = \tilde{t}^{-*} t^-, \qquad (6)$$

where t^- is the column vector of transitions into channel α,

$$t^- = \{t_\alpha^-\} = \{\langle \Psi_{\alpha E} | T | \Psi_i \rangle\}. \qquad (7)$$

An important quantity involved is the CI matrix element between an unmodified resonance state and an unperturbed continuum state $\langle \phi_n | (H - E) | \psi_{\beta E} \rangle = V_{n\beta}$. The wave function of the resonance state ϕ_n is prepared in a valence RCI calculation similar to that for the Ce^- bound states but with two differences. First, the common radial set for Ce I thresholds (as discussed in the previous section) is used to get around the nonorthonormality between the radial functions in ϕ_n and $\psi_{\beta E}$. As in the neutral core of $\psi_{\beta E}$, the second set of virtual orbitals in ϕ_n is optimized separately. However, the radial overlaps between the corresponding radials are always larger than 0.97. It is assumed that the noncorresponding radials are orthogonal. Second, the correlation configurations that are equivalent to the continuum state, i.e., $4f5d6s^2vp$ and $4f5d6s^2vf$, are excluded from the basis set.

For each $V_{n\beta}$, the angular structure of all the R^k and I integrals are generated by the RCI code [31]. One computational difficulty we came across is that our εp is generated orthogonal to the np's ($n \leqslant 6$) but is not orthogonal to the virtual p's. As a result, the value of any radial integral that contains both εp and vp will be erroneous. This is why a diffuse DF $6p$ radial was included in the common radial set. Our intention is that, since this $6p$ radial is similar to that in the resonance state, it will describe the resonance state well enough so that a small correlation effect will be seen from the first virtual p orbital. Following this, two approximations are made to avoid radial integrals involving both $\varepsilon p(f)$ and $vp(f)$ in the angular structure. The first is to use a truncated basis set when calculating the angular structure. Configurations whose coefficients are less than 0.0005 are left out from the basis sets for ϕ_n and the neutral core. The summation of the weights of such configurations in each state is less than 0.1%. Thus, omitting them will cause little change to $V_{n\beta}$. The same strategy was employed in Ref. [32]. The other approximation is to leave out configurations that involve virtual $p(f)$ from the truncated basis set for ϕ_n when evaluating its CI matrix element with a continuum state that contains $\varepsilon p(f)$. The summations of the weights of these configurations are around 2% for virtual p and less than 1% for virtual f. This treatment is acceptable considering our focus is only to qualitatively identify the peaks in the measured neutral signal spectrum.

The radial integrals are evaluated using the continuum integral solver (CIS) code of Perger and Karighattan [33]. A logarithmiclike grid is used to tabulate $V_{n\beta}$ as a function of photon energy. Since all the peaks measured have very narrow widths ($\leqslant 1$ meV to several meV), we make fine steps as small as 0.01 meV around narrow peaks, such as peak E. For $Ce^-\ ^4H_{7/2}$, we have examined 35 relativistic channels of Ce I $4f5d6s^2\ ^1G_4$, $^3F_2$, $^3H_4$, $^3F_3 + \varepsilon p_{1/2,3/2}$, $\varepsilon f_{5/2,7/2}$, with $J_f = 5/2,7/2,9/2$. The computer time of the CIS code increases dramatically for larger photoelectron energies, up to 1.5 h on an AMD 2.4-GHz machine. On average, a tabulation between one resonance state and one continuum state takes 5 h. Usually, three energetically accessible resonance states are mixed into a continuum state. We have worked out a way to speed up the tabulation process. By using a common basis set, the CI matrix elements for the same J_f value will have identical R^k and I radial integrals. Only their angular coefficients differ. Once we have these integrals evaluated for one pair of a resonance state and a continuum state, we can scale them to another pair as long as the J_f is the same. This greatly reduces the tabulation time by a factor of N (N being the number of resonance states considered) and gives us the flexibility to test as many potentially important resonances as necessary.

When plugging Eq. (5) into Eq. (7) to calculate the transition matrix elements, the electric dipole matrix element of the resonance state is extracted from the bound-state code [21,28]. The modification to this matrix element due to the admixture of the continuum states was neglected in Ref. [30] but has been explicitly included here. An estimate for the width of

TABLE III. Resonance transitions involved in each peak in the photodetachment from Ce^- over the energy range of 0.54–0.75 eV. Transitions that either are electric dipole-forbidden or are outside of the photon energy range are labeled as n/a; those that are too weak to produce measurable features are left blank. Resonance states are labeled as Rn, with $R1$ being the lowest-lying resonance state for each J_f.

	Resonance state									
Initial	$J_f = 5/2$	$J_f = 7/2$					$J_f = 9/2$		$J_f = 11/2$		
bound state	$R1$	$R1$	$R2$	$R3$	$R4$	$R5$	$R1$	$R2$	$R1$	$R2$	$R3$
$^4H_{7/2}$	B	C			n/a	n/a	C	E	n/a	n/a	n/a
$^4H_{9/2}$	n/a	r	v	w	n/a	n/a	r	t		s	D
$^4I_{9/2}$	n/a	n/a	B			x		r	n/a		

each resonance peak is performed using Eq. (40) in Ref. [29],

$$\Gamma_n = \Sigma_\beta \Gamma_{n,\beta} = 2\pi \Sigma_\beta v^*_{n,\beta} v_{n,\beta}. \quad (8)$$

The estimated widths for all the calculated peaks fall into two categories: several meV or below 1 meV. They are used to help match the calculated peaks to those in the measurement. Examples will be provided later in this paper.

Our strategy is to plot the cross sections from the lowest-lying Ce^- bound states using an estimated electron affinity (EA). Then, by comparing the calculated peaks to those in the experimental spectrum, we can adjust the EA and make shifts in the resonance states to align the peaks. Since $^4H_{7/2}$, $^4H_{9/2}$, and $^4I_{9/2}$ have some common J_f values, the shifts made for $^4H_{7/2}$ will be carried over to the other two states.

Our previous experimental LPT paper [17] resulted in an EA of 0.65(3) eV. By observing the widths (Table II) and profiles of peaks A (0.618 eV) and B (0.634 eV) (Fig. 2 in the present paper and Fig. 3 in Ref. [17]), we believe that peak B should be an asymmetric shape resonance that lies above the parent neutral state. In other words, the photodetachment threshold should be somewhere between peaks A and B. So, we began with an estimated EA of 0.62 eV and calculated the photodetachment cross section from Ce^- $^4H_{7/2}$, the ground state. All of the resonance states that lie within, or slightly above, the photon energy range have been examined. Three peaks are produced; their relative positions and widths indicate they should be peaks B, C, and E in the experimental spectrum (see Table II), although their positions are 0.014–0.039 eV too high compared to the measured values. The identities of these strong peaks are listed in Table III, where transitions to resonance states that are too weak to produce measurable features are designated as blank entries, and both those outside the photon energy range (e.g., $R4$ and $R5$) and the electric dipole-forbidden $J_f = 11/2$ states are designated as n/a. As shown, peak B is due to the lowest $J_f = 5/2$ resonance state; this $J_f = 5/2$ state was placed at 0.151 eV above its ground state and, therefore, was bound by 0.001 eV in the most recent paper of our group [4]. Estimating the accuracy of RCI to be 0.020 eV, the binding status of this state is actually ambiguous. Usually, the energy difference between states of the same J is obtained from an RCI calculation that optimizes the lowest root. In this paper, we tried to optimize this first excited state, but the RCI calculation failed to converge. This nonconvergence indicates that this state is very likely quasibound, and therefore, it is treated as a resonance state. Later, we find another but smaller component of peak B.

A shift is introduced to align the resonance peaks with the measured positions. The shift is made to the diagonal elements of $4f5d^26s6p$ only. This configuration has a large mixing (see Table IV) in the resonance state $4f5d6s^26p$. It has been correlated equally to $4f5d6s^26p$ in the wave function. However, the missing, but differing, core-valence effect and a radial set that optimizes $4f5d6s^26p$ justify a shift in $4f5d^26s6p$.

Similar calculations are then conducted for Ce^- $^4H_{9/2}$, where peaks r, s, t, D, v, and w are identified (Table III). The BE for $^4H_{9/2}$ was shifted to 0.52 eV to be consistent with the shifted EA of 0.62 eV. It turns out that $^4H_{9/2}$ makes a strong transition to the same resonance state of $4f5d6s^26p$ $J_f = 9/2$, just as $^4H_{7/2}$ does (peak E). The calculated peak lies 0.10 eV lower in energy than peak E, equal to the gap between Ce^- $^4H_{7/2}$ and $^4H_{9/2}$. However, in the measured spectrum, there are two peaks at this position, t and u, which almost

TABLE IV. Calculated positions of the resonance peaks before and after a shift is made to $4f5d^26s6p$ in each resonance state. All units are in meV.

Peak		No shift	Shift		
Label	J_f	Position	Position	Change[a]	$4f5d^26s6p$
r	7/2	574	557	−17	29%
	9/2	576[b]	556	−20	31%
	9/2	592[c]	554	−38	35%
s	11/2	571			22%
t	9/2	636[c]	597	−39	35%
B	5/2	657	636	−21	23%
	7/2	664[d]	636	−28	71%
C	7/2	672	654	−18	29%
	9/2	674	654	−20	31%
D	11/2	733	665	−68	68%
v	7/2	708	680	−28	71%
E	9/2	734	695	−39	35%
w	7/2	728	710	−18	36%
x	7/2	775	734	−41	49%

[a]Change compares to the peak position with no shift.
[b]Inferred from peak C, which corresponds to the same resonance state but from $^4H_{7/2}$.
[c]Inferred from peak E, which corresponds to the same resonance state but from $^4H_{7/2}$.
[d]Inferred from peak v, which corresponds to the same resonance state but from $^4H_{9/2}$.

overlap with an energy difference of only 0.25 meV. The final designation is facilitated by realizing that the peak should have a very similar width to that of E as they correspond to the same upper resonance state. The experimentally measured width of peak t is almost identical to E (Table II), whereas, peak u is a factor of 2 wider; therefore, we conclude that this calculated peak should correspond to the peak labeled as t in the experimental spectrum. Finally, the photodetachment cross sections from the second excited Ce^- state $^4I_{9/2}$ are calculated where new components of peaks B and r and a new peak x are identified.

At this stage, we have identified all the peaks in the experimental spectrum except for peaks u (at 0.600 eV) and A (at 0.618 eV), using an EA of 0.62 eV and binding energies of 0.52 eV ($^4H_{9/2}$) and 0.486 eV ($^4I_{9/2}$). Both peaks u and A have narrow widths and lie slightly below the detachment threshold. We believe that they are bound-bound transitions from the Ce^- $^4H_{7/2}$ ground state to even-parity $4f5d6s^26p$ states. By referring to the binding energies of Ce^- (Table I), the only possible candidates are the two least-bound states: $4f5d6s^26p\ ^2H_{9/2}$ and $4f5d6s^26p\ ^2F_{7/2}$. In this paper, RCI calculations for these two states were conducted again where $4f5d^26s6p$ was correlated equally to $4f5d6s^26p$ due to its large weight (∼17%) in the wave function. It was found that transitions from Ce^- $^4H_{7/2}$ into these states have f values on the same order of magnitude as the large ones in Table III of Ref. [14]: 1.33×10^{-4} (Babuskin gauge) for $^2H_{9/2}$ and 3.94×10^{-4} (Coulomb gauge) for $^2F_{7/2}$. The specific gauge is selected because it remains stable as small variations are made in the calculations. At this stage, it became obvious that the EA we had been using was too small to account for the transition energies of these two peaks. Therefore, we increased it to 0.628 eV in order to match the measured 0.600-eV transition energy into $4f5d6s^26p\ ^2F_{7/2}$ that produced peak u. The BE of $4f5d6s^26p\ ^2H_{9/2}$ needs to be shifted from 0.018 to 0.010 eV in order to account for the transition energy of 0.618 eV for peak A. Again, this small change of 0.008 eV in its BE falls within the reasonable accuracy of 0.020 eV for RCI calculations.

With the new EA of 0.628 eV, the BE of $^4H_{9/2}$ is shifted accordingly to 0.530 eV to match the energy difference of 0.098 eV between peaks t and E. The BE for $^4I_{9/2}$ remains at 0.486 eV so that it is of the same energy value above $^4H_{9/2}$ (see Table I). Next, a new cycle of calculations was carried out where adjustments to the amount of shift to $4f5d^26s6p$ were made to align the peaks. Depending on the resonance, the amount of shift varies between 0.05 and 0.20 eV.

IV. RESULTS AND DISCUSSION

A. Comparison of experiment and theory

The resonance transitions from $^4H_{7/2}$, $^4H_{9/2}$, and $^4I_{9/2}$ are summarized in Table III. In Table IV, we summarize the positions of the peaks before and after a shift is made to $4f5d^26s6p$ in the resonance state. Column 3 shows that even before the shift, the order of the large peaks t, B, C, D, and E agrees with the measurement. Column 5 shows that shifting $4f5d^26s6p$ lowers the peaks by 0.017–0.068 eV. However, these varying amounts do not alter the order of those large peaks. One may notice that, before the shift, peak C was very close to the measured peak D. However, its estimated width was about 7 meV, which is on the same order of magnitude as the measured width for peak C of 2.8 meV but is 2 orders of magnitude larger than the measured width for peak D of 0.099 meV. This helps justify our designation of it as peak C and the use of the shift to bring it into position. Its width after the shift is about 2 meV, which is consistent with the measured width.

The composition of $4f5d^26s6p$ in a resonance state affects how much the resonance peak is lowered by a shift in $4f5d^26s6p$. An example of this can be found in peaks D and E, which are due to the detachment from $^4H_{9/2}$ and $^4H_{7/2}$, respectively. Without the shift in $4f5d^26s6p$, the two peaks are only 0.001 eV apart (column 3) and almost overlap. When an almost identical shift was made to $4f5d^26s6p$ in the resonance state, peak D was lowered by 0.068 eV while peak E was lowered by 0.039 eV due to the much larger amount of $4f5d^26s6p$ in the former than in the latter (column 6). The two peaks are now well separated, with peak E clearly being due to the detachment from $^4H_{7/2}$. There is further evidence based on the energy separation of the two lowest bound states of Ce^- that supports this identification of peak E. Ce^- $^4H_{7/2}$ and $^4H_{9/2}$ both have a strong transition into the same $J_f = 9/2$ resonance state (Table III), producing large resonance peaks. The energy gap between these two peaks should then be equal to the difference in the binding energies, i.e., 0.098 eV. Given that the peak from $^4H_{9/2}$ lies at 0.600 eV (peak t), the peak from $^4H_{7/2}$ should then lie at about 0.698 eV, which is peak E.

The final calculated peak positions are compared to the measured peak energies in Table II. The general agreement between the measured and the calculated positions is very good, with discrepancies of only 0.000–0.006 eV. The calculated photodetachment cross section in the Coulomb gauge is shown in Fig. 2 together with the measured neutral signal spectrum. Theoretically, the Babuskin gauge and the Coulomb gauge should give identical results. However, with an approximate wave function, their difference is rooted in all methodologies except for the relativistic random-phase approximation method [34]. In this paper, the Babuskin gauge of the transition matrix elements for the continuum states abnormally fluctuate toward the high-photon energy tail; therefore, we use the Coulomb gauge instead. In a computational study for photodetachment of C^-, the nonrelativistic velocity gauge was found to agree well with the experiment [32].

The cross section plot in Fig. 2 is generated by adding the cross sections from $^4H_{7/2}$, $^4H_{9/2}$, and $^4I_{9/2}$ with a multiplicative coefficient for each state based on Boltzmann distributions. We assume that the ion beams were populated mostly by the ground state, and an effective temperature of 650 K was used for the Boltzmann factor, which gave the best qualitative similarity of the calculated spectrum to the measured result. This assumed temperature is at the low end of typical effective temperatures in sputter-ion sources. However, since the ion beam was very likely not in thermal equilibrium, more quantitative comparisons are not productive. Peaks u and A are due to the two-step process discussed earlier, with a resonant transition between bound states followed by photodetachment. Their amplitudes should be the photodetachment cross sections from the excited states when each absorbs an identical photon and detaches. An investigation into the absolute magnitudes of these cross sections falls outside the

goal of this paper but will be studied in a separate calculation. In the simulated plot of Fig. 2, peaks u and A, respectively, are represented by two Gaussian functions with the full width at half maximum being equal to the measured width in Table II. Arbitrary amplitudes are assigned to the Gaussian functions as our purpose is to indicate their positions in the spectrum only.

Both the measured and calculated spectra in Fig. 2 show a gradual rise in the continuum cross section above $\sim$0.65 eV due to the p-wave thresholds for photodetachment from the ground state of Ce^- to the two lowest neutral Ce states. All of the peaks in the measured spectrum are reproduced in the calculations. The calculated relative amplitudes of peaks C, D, and E qualitatively agree very well with the measurements. Detailed quantitative comparisons are precluded by the unknown composition of the initial states of the ions in the beam. Moreover, the relative amplitudes and widths determined by the theoretical calculations are used only to facilitate the identification of the peaks. Differences between the calculated and measured peak amplitudes and widths are mainly due to the exact positioning of the resonance states and the mixing of the $4f5d^26s6p$ component in the resonance states as illustrated below for the examples of peak B and peak r.

The relative amplitude of calculated peak B appears to be substantially larger than in the measurement, and some interesting phenomena happen when we calculate the amplitude for peak B. As shown in Table III, peak B consists of two components: the first is due to the transition from $^4H_{7/2}$ to the $J_f = 5/2$ resonance state, and the second is due to the transition from $^4I_{9/2}$ to a $J_f = 7/2$ resonance state. It is the first component that produces a very large cross section; the second component is wider, but it disappears into the first component due to its small cross section. The $J_f = 5/2$ resonance state is very close to the neutral threshold. It is known that a shape resonance close to threshold appears asymmetrical [6,35–38] and, therefore, should have a small line-shape parameter. The reported line-shape parameter for peak B in Ref. [17] is the smallest among all of the observed peaks, which is consistent with its being a shape resonance near the threshold. Without shifting $4f5d^26s6p$, the first component of peak B is found to lie at 0.657 eV, coinciding with the turn-on of the Ce I $^3F_2$ threshold. To align it with the measured peak B, a shift of 0.124 eV was introduced, which lowers the resonance state by 0.021 eV. However, the resonance peak was lowered to 0.649 eV—a change of only 0.008 eV. A more aggressive shift of 0.204 eV was made, which brought down the resonance peak to 0.636 eV, in good agreement with the measured value of 0.634 eV. But then, the amplitude of the peak increases dramatically from 3.0 Mb (at 0.649 eV) to 31.2 Mb (at 0.636 eV). Meanwhile, the estimated width of the peak decreases from 1.9 to 0.5 meV, while the measured width is 2.5(5) meV. So it appears that the better we position the peak, the less it resembles the measured peak. A direct reason for this is that the resonance state has a composition of about 20% of $4f5d^26s6p$, which is a Feshbach resonance configuration that lies below the parent state of Ce I $4f5d^26s$ and produces a narrower width than shape resonances. This configuration enables a strong $6s \rightarrow 6p$ transition from Ce^- $4f5d^26s^2$. Shifting it increases its composition in the resonance state. As a result, the combined cross section increases, but the width of the resonance peak decreases. This indicates that our positioning of $4f5d6s^26p$ is not accurate, and the error is not solely due to the proper mixing of $4f5d^26s6p$. The sources of the error could be the common radial set used for all states and the inadequacy of the correlation effect. However, since the error is less than 0.015 eV—which is reasonable accuracy for RCI calculations—and our main objective is to identify the peaks in the measured spectrum, we are content with positioning the peak at 0.636 eV.

The calculated peak r is narrower than measured. This peak consists of three separate transitions as shown in Table III. The two peaks produced by $^4H_{7/2}$ and $^4H_{9/2}$ have similar widths of about 5 meV and are very close to each other. A small change in the amount of the shift would have separated them by several meV and would have resulted in peak r being wider. Another reason is that there might be resonance transitions from higher-lying Ce^- bound states that are superimposed on peak r.

B. Electron affinity and fine structure

The electron affinity of Ce is determined in the present paper through the observation and identification of two resonance peaks that straddle the neutral ground-state photodetachment threshold, both of which are due to transitions from the Ce^- $^4H_{7/2}$ ground state. Peak A at 0.618 16(3) eV is identified as due to a bound excited state of the negative ion lying below the neutral Ce ground state, while peak B at 0.6338(4) eV is due to a quasibound resonance state lying just above the neutral Ce ground state. Thus, the threshold must lie between peaks A and B as shown in Fig. 2. Therefore, based on the experimental results and the theoretical analysis, we recommend a value of 0.628(10) eV for the electron affinity of Ce with the uncertainty based on the energy separation between these two peaks.

The present electron affinity is compared to previous experimental and theoretical values in Table V. The present value is consistent with our previous experimental value of 0.65(3) eV obtained through measurement of the detachment threshold for the Ce^- ($^4H_{7/2}$) to Ce ($^1G_4$) ground-state to ground-state transition [17]. The smaller uncertainty in the present paper is due to the sharper resonance features used to bracket the threshold as opposed to the previous use of the weak p-wave detachment behavior, which has zero slope at the threshold. The strengths of the resonance features and the significant background due to detachment from more weakly bound states make determination of the threshold energy challenging. The present result is also in good agreement with recent calculations of 0.61 eV by Felfli *et al.* [15] and of 0.58(10) eV by Cao and Dolg [5]. Although the LPES experiment by Davis and Thompson yielded a much higher electron affinity of 0.955(26) eV [16], the subsequent reinterpretation of the LPES data by O'Malley and Beck determined an electron affinity of 0.660 eV [14], which is consistent with the present result.

The fine structure splitting of the ground state of Ce^- ($^4H_{7/2}$-$^4H_{9/2}$) is determined to be 0.097 75(4) eV based on the measured energy difference between peaks t and E, which are due to excitation of the same upper state from these two different lower states of the negative ion (Table III). This value is in excellent agreement with the RCI calculation by O'Malley and Beck of 0.100 eV based on the difference between the binding energies of $^4H_{7/2}$ (0.660 eV) and $^4H_{9/2}$

TABLE V. Comparison of the present results for the electron affinity of Ce to selected previous measurements and theoretical calculations. Methods – Experimental: LPT and LPES; Theoretical: RCI; RP, Regge-pole analysis; and MRCI, pseudopotential multireference configuration interaction.

Reference	Method	Electron affinity (eV)
Present paper	LPT + RCI	0.628(10)
Felfli *et al.* (2009) [15]	RP	0.61
Walter *et al.* (2007) [17]	LPT	0.65(3)
O'Malley and Beck (2006) [14]	RCI reinterpretation of LPES	0.660
O'Malley and Beck (2006) [14]	RCI	0.511
Cao and Dolg (2004) [5]	MRCI	0.58(10)
Davis and Thompson (2002) [16]	LPES	0.955(26)
O'Malley and Beck (2000) [13]	RCI	0.428

(0.560 eV) [4]. It is also consistent with the MRCI calculation by Cao and Dolg of the energy difference between these two states of 0.109 eV [5]. The separation between $^4H_{9/2}$ and $^4I_{9/2}$ is determined to be 0.046(5) eV based on the measured energy difference between peaks v and B or between t and r. The uncertainty is dominated by the multiple component transitions in peaks B and r. This measured value is in very good agreement with the calculation by O'Malley and Beck of 0.044 eV for the ($^4H_{9/2}$–$^4I_{9/2}$) separation [4].

C. Bound-bound transitions

Two transitions between bound states of Ce^- are observed in the present paper through two-step processes: peak u at 0.600 23(3) eV is due to the transition $4f5d^26s^2\ ^4H_{7/2} \rightarrow 4f5d6s^26p\ ^2F_{7/2}$, and peak A at 0.618 16(3) eV is due to the transition $4f5d^26s^2\ ^4H_{7/2} \rightarrow 4f5d6s^26p\ ^2H_{9/2}$. In both cases, the excited state subsequently absorbs a second photon to detach an electron from the negative ion. Thus, Ce^- is only the second negative ion confirmed to have bound states of opposite parity for which electric dipole transitions are allowed. The other example, Os^-, was also first observed through a similar photodetachment process [6].

Since peaks u and A are due to two-step processes, the photodetachment signal should depend quadratically on the laser-pulse energy in the nonsaturated regime. However, we have not been able to observe deviation from linear one-photon behavior in the present experiments, because the significant component of background signal due to direct photodetachment of more weakly bound ions in the beam obscures the possible two-photon behavior.

V. CONCLUSIONS

To summarize, our study of Ce^- combining experimental tunable laser photodetachment and calculations of the cross sections, including bound and quasibound excited states, has refined the electron affinity of Ce to be 0.628(10) eV. The fine structure splitting of the ground state of Ce^- ($^4H_{7/2}$–$^4H_{9/2}$) is measured to be 0.097 75(4) eV; thus, the BE of the first excited state of Ce^- ($^4H_{9/2}$) is 0.530(10) eV. The rest of the binding energies of odd states of Ce^- in Ref. [4] can be adjusted by a uniform decrease of 0.032 eV for $J = 7/2$ and 0.030 eV for $J = 9/2$. In addition, two bound-bound electric dipole transitions have been observed in Ce^-, confirming that it has multiple bound states of opposite parity. The present paper highlights the uniqueness of cerium and its negative ion, showing an unprecedented density of bound and low-lying resonance states. The paper further demonstrates the power of combined experimental and theoretical approaches to gain insight into complex many-body systems, such as the lanthanides.

ACKNOWLEDGMENTS

This material is based, in part, upon work supported by the National Science Foundation under Grant No. PHY-0757976. Y.-G.L., D.J.M., R.M.A., and S.E.L. received partial support from Denison University's Anderson Summer Research Fund. D.H. acknowledges support from the Swedish Research Council and Denison University. L. Pan and D. R. Beck acknowledge support from the National Science Foundation, Grant No. PHY-0652844.

[1] D. J. Pegg, Rep. Prog. Phys. **67**, 857 (2004).
[2] T. Andersen, H. K. Haugen, and H. Hotop, J. Phys. Chem. Ref. Data **28**, 1511 (1999).
[3] T. Andersen, Phys. Rep. **394**, 157 (2004).
[4] S. M. O'Malley and D. R. Beck, Phys. Rev. A **79**, 012511 (2009).
[5] X. Cao and M. Dolg, Phys. Rev. A **69**, 042508 (2004).
[6] R. C. Bilodeau and H. K. Haugen, Phys. Rev. Lett. **85**, 534 (2000).
[7] U. Warring, M. Amoretti, C. Canali, A. Fischer, R. Heyne, J. O. Meier, Ch. Morhard, and A. Kellerbauer, Phys. Rev. Lett. **102**, 043001 (2009).
[8] A. Fischer, C. Canali, U. Warring, A. Kellerbauer, and S. Fritzsche, Phys. Rev. Lett. **104**, 073004 (2010).
[9] A. Kellerbauer and J. Walz, New J. Phys. **8**, 45 (2006).
[10] S. M. O'Malley and D. R. Beck, Phys. Rev. A **81**, 032503 (2010).
[11] L. Pan and D. R. Beck, Phys. Rev. A **82**, 014501 (2010).

[12] Y. Ralchenko *et al.*, NIST Atomic Spectra Database (version 4), available at [http://physics.nist.gov/pml/data/asd.cfm], National Institute of Standards and Technology, Gaithersburg, MD, 2009.
[13] S. M. O'Malley and D. R. Beck, Phys. Rev. A **61**, 034501 (2000).
[14] S. M. O'Malley and D. R. Beck, Phys. Rev. A **74**, 042509 (2006).
[15] Z. Felfli, A. Z. Msezane, and D. Sokolovski, Phys. Rev. A **79**, 012714 (2009).
[16] V. T. Davis and J. S. Thompson, Phys. Rev. Lett. **88**, 073003 (2002).
[17] C. W. Walter, N. D. Gibson, C. M. Janczak, K. A. Starr, A. P. Snedden, R. L. Field III, and P. Andersson, Phys. Rev. A **76**, 052702 (2007).
[18] C. W. Walter, N. D. Gibson, D. J. Carman, Y.-G. Li, and D. J. Matyas, Phys. Rev. A **82**, 032507 (2010).
[19] Y. Saitoh, B. Yotsombat, K. Mizuhashi, and S. Tajima, Rev. Sci. Instrum. **71**, 955 (2000).
[20] U. Fano, Phys. Rev. **124**, 1866 (1961).
[21] D. R. Beck, Phys. Scr. **71**, 447 (2005).
[22] J. P. Desclaux, Comput. Phys. Commun. **9**, 31 (1975).
[23] S. M. O'Malley and D. R. Beck, Phys. Rev. A **77**, 012505 (2008).
[24] W. F. Perger, Z. Halabuka, and D. Trautmann, Comput. Phys. Commun. **76**, 250 (1993).
[25] M. G. Tews and W. F. Perger, Comput. Phys. Commun. **141**, 205 (2001).
[26] R. D. Cowan, *The Theory of Atomic Structure and Spectra* (University California Press, Berkeley, CA, 1981), p. 525.
[27] D. R. Beck, program RPI (unpublished).
[28] D. R. Beck, program RFV (unpublished).
[29] F. H. Mies, Phys. Rev. **175**, 164 (1968).
[30] L. Pan and D. R. Beck, J. Phys. B **43**, 025002 (2010).
[31] D. R. Beck, program RCI (unpublished).
[32] N. Miura, T. Noro, and F. Sasaki, J. Phys. B **30**, 5419 (1997).
[33] W. F. Perger and V. Karighattan, Comput. Phys. Commun. **66**, 392 (1991).
[34] W. R. Johnson and C. D. Lin, Phys. Rev. A **20**, 964 (1979).
[35] C. W. Walter and J. R. Peterson, Phys. Rev. Lett. **68**, 2281 (1992).
[36] J. R. Peterson, Y. K. Bae, and D. L. Huestis, Phys. Rev. Lett. **55**, 692 (1985).
[37] C. W. Walter, J. A. Seifert, and J. R. Peterson, Phys. Rev. A **50**, 2257 (1994).
[38] C. W. Walter, N. D. Gibson, R. C. Bilodeau, N. Berrah, J. D. Bozek, G. D. Ackerman, and A. Aguilar, Phys. Rev. A **73**, 062702 (2006).